SIN-CHN
SCIENTIFIC PRESS PTE.LTD.

Molecular & Cellular Biomechanics 2024, 21(1), 277.
https://doi.org/10.62617/mcb.v21i1.277

Article

Three-dimensional finite element analysis of biological signal feedback in the mechanical properties of sound production

Jiarong Liu

College of Music and Dance, Hunan First Normal University, Changsha 410205, Hunan, China; ljr391037@hnfnu.edu.cn

CITATION

Liu J. Three-dimensional finite element analysis of biological signal feedback in the mechanical properties of sound production. Molecular & Cellular Biomechanics. 2024; 21(1): 277.
https://doi.org/10.62617/mcb.v21i1.277

ARTICLE INFO

Received: 23 July 2024
Accepted: 13 September 2024
Available online: 22 October 2024

Abstract: In response to the problems of low reliability and long time consumption in traditional research on sound production, this article used electromyography (EMG) signals as input signals to build a high-precision sound production mechanics model. A Proportional-Integral-Derivative (PID) controller was used to dynamically adjust the model and develop a real-time feedback system. This article established a detailed three-dimensional (3D) finite element model including the vocal cords and throat, defined the nonlinear elastic properties and linear elastic properties of different tissues, and used tetrahedral grid partitioning technology to improve the computational accuracy of the model. Through a EMG sensor, an individual EMG was collected and filtered to remove noise. The processed EMGs were used as input parameters for the finite element model to drive the muscle units in the model. By using a PID controller to receive real-time EMG input, the error was calculated and the model was adjusted, enabling accurate simulation of the mechanical properties of vocal cord vibration under different vocal states and achieving real-time feedback. Considering the complexity of vocal cord vibration driven by biological signals, this article simulated and analyzed the modal characteristics of vocal cord vibration, and analyzed the differences in vocal cord vibration characteristics under different vocal states. The sound pressure distribution and resonance frequency were simulated and analyzed to understand the propagation characteristics of sound. Finally, by comparing and analyzing the simulated data with the actual collected data, it was found that the maximum relative error rate of the model under different sound states was 6.14%, and the overall error rate of the model was relatively low, which verified the reliability of the model. The findings demonstrated that the feedback delays of the model in different sound states were all within 100 milliseconds, indicating that the system had high real-time performance and accuracy, which was promising in practical applications.

Keywords: three-dimensional finite element analysis; biological signal feedback; mechanical properties; PID controller; vocal cord vibration

1. Introduction

As technology has developed in recent years, the study of sound production mechanisms has become more and more in-depth. The study of sound production mechanisms is important in many fields (including biomechanics, acoustics and medicine) [1–3]. In this article, a 3D finite element model is constructed and individual biosignals are applied into the acoustic model [4–6] to enhance the accuracy and applicability of the model.

Finite element analysis [7–9] is a broadly utilized analytical method in biomechanical and acoustic studies for simulating and analyzing the mechanical behavior of complex structures. Within the research of sound vocalization, finite element analysis is used to construct a 3D model of the vocal cords to study the mechanical properties of vocal cord vibration, sound wave propagation, and sound

pressure distribution [10,11]. Most of the early studies were carried out using simplified models and low-resolution grids, making the accuracy of model simulations and the effectiveness of practical applications less than ideal. By applying high-density grids and more accurate linear and nonlinear elastic models [12,13], the accuracy and reliability of three-dimensional finite element model simulation are greatly improved, which also enables it to play a significant role in practical applications.

Biosignal acquisition and processing is one of the key steps in constructing high-precision acoustic models [14−16]. The common biological signal used for sound production research is EMG [17−19], which can directly capture the electrical activity of the vocal cords and related muscles, providing more accurate sound production data. After signal acquisition, EMG is usually preprocessed to remove noise and interference [20,21].

Real-time control and dynamic adjustment are key technologies for achieving high-precision sound simulation [22,23], which can significantly improve the adaptability and accuracy of the model. PID controller, as a classic real-time control algorithm [24−26], is widely used in industrial automation and process control, and is often used in the construction of real-time feedback systems.

This article proposes a three-dimensional finite element acoustic dynamics model based on biological signal feedback. By applying high-precision EMG acquisition and processing technology, combined with PID controller to achieve real-time dynamic adjustment, a vocal cord vibration model with real-time feedback capability is constructed. The experimental findings demonstrate that the model has high accuracy and real-time performance, and can be effectively used for personalized medical diagnosis and treatment, which has a broad application prospect.

2. Related work

Traditional studies of sound production are usually grounded on idealized geometrical structures in two or three dimensions [27−29]. These research methods are difficult to accurately reflect the dynamic changes in individual physiological characteristics and vocal states [30,31]. In recent years, significant progress has been made in the study of sound production mechanisms, and many researchers have made relevant research results. Jiang W [32] et al. conducted a study on the influence of vocal cord cover thickness on vocal cord vibration and vocalization, analyzing the impact of cover thickness on vibration dynamics during vocalization from multiple perspectives such as fundamental frequency, characteristic frequency, and characteristic mode. Zhang Z [33] studied the oral vibration during speech production under different throat and semi-occluded channel configurations. During the study, a three-dimensional speech model was used to quantify the oral sound pressure level (SPL) and make adjustments to speech therapy under different semi-occluded channel configurations. The research ideas of the above studies provided reference for the research of this article. Many researchers have also made relevant research summaries in the field of biological signals. Sharma A [34] et al. explored the application scenarios of EMG signals and proposed that time-frequency analysis should usually be used when EMG signals are used for clinical evaluation. The time-frequency

analysis in the research process involves converting signals in different domains and extracting useful physiological information. This study provided a theoretical basis for this article.

In sound generation simulation, the PID controller can receive real-time feedback from biological signals, continuously adjust the parameters and boundary conditions of the sound generation model, ensure the consistency between the model output and the actual biological signals, and maintain the dynamic response capability of the model. There are also many researchers involved in the field of combining finite element analysis with PID controllers for research. Kamel M A [35] et al. developed a new vibration control dynamic model through finite element analysis. This study conducted frequency analysis (modal and harmonic) on the model and combined it with a PID controller to achieve an intelligent controller system with good system performance. Guan W [36] et al. proposed a mathematical modeling method for lumbar spine deformation based on finite element simulation using response surface methodology. This experiment was based on CT (Computed Tomography) scan data, reconstructed a three-dimensional model of the lumbar spine including vertebral bodies and intervertebral discs, and used finite element method to analyze the lumbar spine. Based on simulation results, relevant mathematical models were established and PID controllers were combined to construct a position control system. The effectiveness of the mathematical model was verified through simulation and comparative experiments on the control system. The above research provided a more specific research approach for this article.

Based on the above research, by applying EMG as input, combined with finite element analysis and real-time control technology, a high-precision and dynamically responsive vocal model was ultimately constructed. These studies not only enhanced the theoretical understanding of vocalization mechanisms, but also provided new methods and means for personalized medical diagnosis and treatment.

3. Specific implementation of three-dimensional finite element analysis

3.1. Construction of 3D finite element model

To realize 3D finite element analysis of the mechanical properties of sound production, it is necessary to first construct accurate three-dimensional finite element models of the vocal cords and throat. High-resolution CT scans and MRI (Magnetic Resonance Imaging) data are used to obtain geometric information of the vocal cords and larynx. CT scans can provide density information of bones and soft tissues, while MRI can provide more detailed structural information of soft tissues. CT and MRI data are subjected to denoising, smoothing, and segmentation processing. The segmentation process extracts the vocal cords and throat from surrounding tissues, generating a 3D contour of the target area. The segmented data is utilized for surface reconstruction, generating three-dimensional surface models of the vocal cords and throat. The generated surface model needs to be smoothed to remove artifacts and noise generated during the reconstruction process. The model is illustrated in **Figure 1**.

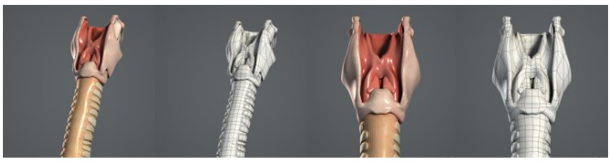

Larynx 3D model

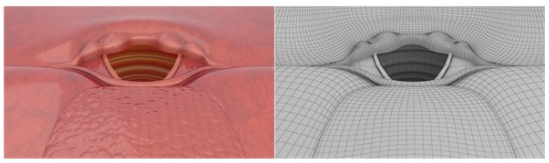

Vocal cord 3D model

Figure 1. Three-dimensional geometric model of throat and vocal cord.

In order to accurately describe the mechanical behavior of materials during stress and deformation, material properties are defined. The vocal cords and other parts of the throat are composed of various types of tissues, such as muscles, mucous membranes, and cartilage. Different organizations have different mechanical properties and exhibit different responses under the same conditions. By defining material properties, these specific responses can be simulated. The collected CT and MRI data is classified based on tissue density and magnetic resonance signal intensity. For muscle tissue, the Ogden model is used to describe its nonlinear elastic behavior. The Ogden model is a more general nonlinear elastic model that is applicable to a wider range of materials, including some complex biological tissues. It flexibly describes the nonlinear behavior of materials through a series of parameters, as shown in Equation (1).

$$W = \sum_{i=1}^{N} \mu_i \alpha_i \left(\lambda_1^{\alpha_i} + \lambda_2^{\alpha_i} + \lambda_3^{\alpha_i} - 3\right) \tag{1}$$

Among them, W is the strain energy function. μ_i and α_i are the material parameters of the Ogden model. λ_1, λ_2 and λ_3 are the principal strains, representing the deformation of the material in three main directions.

For cartilage tissue, a linear elastic model is used to describe its mechanical properties. The stress-strain equation shown in Equation (2) is used to describe the relationship between the stress generated by a material under strain, which is the constitutive equation of a linear elastic material.

$$\sigma_{ij} = C_{ijkl} \epsilon_{kl} \tag{2}$$

Among them, σ_{ij} is stress, describing the internal forces of the material. C_{ijkl} is the elastic constant (or material stiffness matrix), which describes the mechanical properties of the material. ϵ_{kl} is strain, describing the degree of deformation of the material.

Through the application of the above models, accurate simulation of biological tissues can be achieved, providing a foundation for personalized medical diagnosis and treatment.

After completing the definition of material properties, grid division is carried out to partition the continuum into a finite number of small cells, and approximate

calculations are carried out within each cell, thus improving the overall calculation accuracy. In addition, grid partitioning can better capture the details of complex geometric structures, improve the accuracy of simulations, and minimize the consumption of computing resources while ensuring computational accuracy, thus improving computational efficiency.

This article adopts adaptive grid partitioning technology to adjust grid density according to the complexity of geometric shapes. By using the dynamic equation shown in Equation (3), the dynamic response of the vocal cords and throat under external forces such as airflow pressure and muscle drive is described.

$$M\ddot{u} + C\dot{u} + Ku = f \tag{3}$$

The finite element model is validated through experimental data. According to the verification results, the model parameters are adjusted. The material properties, boundary conditions, and grid density are optimized to ensure that the model accurately reflects the mechanical behavior of the vocal cords and throat. Through repeated verification and adjustment, a high-precision three-dimensional finite element model is established.

3.2. Biological signal acquisition and processing

To realize a 3D finite element model driven by biological signals, high-precision collection and processing of the individual EMG are required. Firstly, high-quality surface electrodes or insertion electrodes are used to capture the electrical signals generated by muscle activity. Then, differential amplification technology is employed to improve the signal-to-noise ratio and reduce common mode noise caused by electromagnetic interference or other external sources. Next, a bandpass filter with a frequency range of 20 Hz to 500 Hz is applied to remove irrelevant low-frequency and high-frequency noise. After signal digitization, data smoothing is used for further denoising. **Figure 2** is a schematic diagram of signal acquisition.

This article uses a highly sensitive and high signal-to-noise ratio Surface Electromyography (sEMG) sensor, branded Delsys Trigno series, as shown in **Figure 2a**. Based on anatomical knowledge, sEMG sensors are placed on the surface of vocal related muscle groups. In this study, EMG signals are collected on the surfaces of the left and right sternocleidomastoid and cricothyroid in the throat. The positions of the left and right sternocleidomastoid and cricothyroid in the human body are shown in **Figure 2b,c**, respectively, and the placement position of the sEMG sensor is shown in **Figure 2d**. During the placement of sensors, cleaning and exfoliating treatments are used to reduce the resistance between the skin and electrodes, thereby improving signal transmission efficiency. The skin is cleaned with alcohol swabs to ensure good contact between the electrodes and the skin.

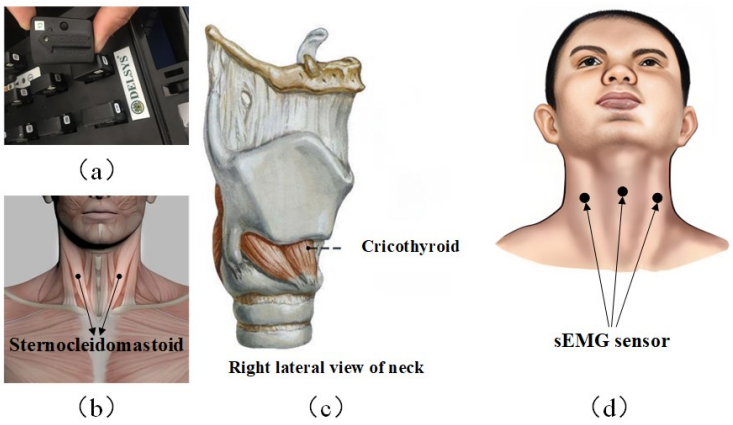

Figure 2. Schematic diagram of signal acquisition. **(a)** represents a Delsys Trigno series brand; **(b)** represents the position of the left and right sternocleidomastoid muscles in the human body; **(c)** represents the position of the cricothyroid membrane in the human body; and **(d)** represents the placement position of the sEMG sensor.

The sampling frequency is set to 1000 Hz during the signal acquisition setup phase to ensure sufficient EMG details are captured. During the collection process, participants are required to perform a series of standardized vocal tasks and record electromyographic signals under different vocal states. From the perspective of vocal continuity, vocal states can be classified into three types: Single Syllable, Speech, and Singing. The signals collected on the surfaces of the left sternocleidomastoid (Left SCM), right sternocleidomastoid (Right SCM), and cricothyroid are shown in **Figure 3**, indicating a significant difference in continuity.

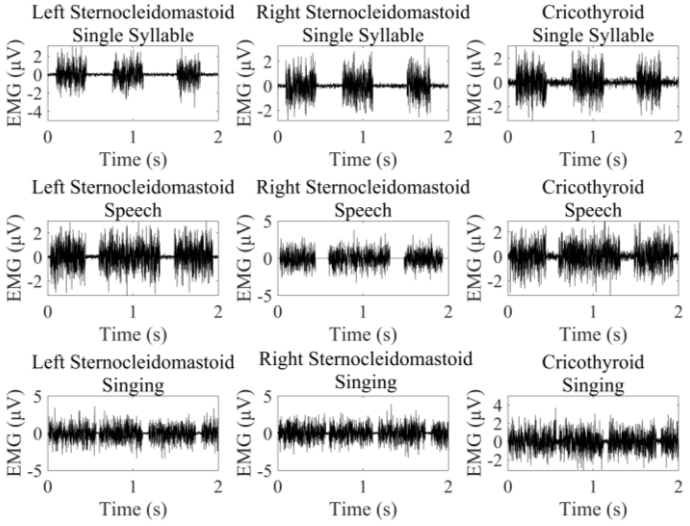

Figure 3. Diagram of EMG under different vocal states

The collected raw EMG are subjected to signal processing, which is a crucial step in converting the collected raw EMG into inputs that can be used for finite element models.

Due to the weak and noisy sEMG signals collected, signal amplification and filtering are required. A differential amplifier is used to preliminarily amplify the signal, and a bandpass filter (such as 20 Hz to 500 Hz) is used to remove low-

frequency noise and high-frequency interference. The specific filter design is shown in Equation (4).

$$H_{bp}(\mathrm{s}) = \frac{\omega_h s}{s^2 + (\omega_h + \omega_\mathrm{l})s + \omega_h \omega_l} \tag{4}$$

Among them, ω_h and ω_l are the high-frequency and low-frequency cutoff frequencies, respectively, and s is the complex frequency variable.

At the same time, a notch filter is used to remove power frequency interference (such as 50 Hz or 60 Hz), and the notch filter design is shown in Equation (5).

$$H_{br}(s) = \frac{s^2 + \omega_0^2}{s^2 + \omega_b \mathrm{s} + \omega_0^2} \tag{5}$$

Among them, ω_0 is the center frequency of the power frequency; ω_b is the width of the stopband; s is a complex frequency variable. The design parameters of the pass filter and notch filter are shown in **Table 1**:

Table 1. Filter design parameters.

Parameter	Band-pass filter	Notch filter
Lower Cutoff Frequency	20 Hz	-
Higher Cutoff Frequency	500 Hz	-
Center frequency	-	50 Hz
Bandwidth	480 Hz	2 Hz
Order	4th order	2nd order

Finally, wavelet transform is used to further remove residual noise. Wavelet transform can perform multi-scale analysis on signals in the time-frequency domain, effectively separating signals and noise. EMG signals are usually non-stationary, and their statistical characteristics vary over time. Wavelet transform is adaptive and can automatically adjust the size of the analysis window based on the local characteristics of the signal. It also allows for multi-resolution analysis, which involves observing the signal at different scales. This multi-scale analysis helps distinguish different features in the signal. The choice of wavelet basis will affect the time-frequency characteristics of the decomposition results. The choice of threshold directly affects the denoising effect. A threshold that is too low can result in excessive noise residue, while a threshold that is too high may delete some useful information from the signal. For electromyographic signals, wavelet bases with good time localization and frequency localization are usually selected. Appropriate wavelet bases for multi-level decomposition of signals are selected to obtain detail coefficients and approximation coefficients at different scales. The detail coefficients are subjected to threshold processing to achieve the effect of removing noise components. The commonly used threshold processing methods include hard threshold and soft threshold processing. In this article, soft threshold processing is adopted, as shown in Equation (6). The processed detail coefficients and approximation coefficients are subjected to inverse wavelet transform to reconstruct the denoised signal.

$$d_i{}' = \mathrm{sign}(d_i) \cdot \max(|d_i| - \lambda, 0) \tag{6}$$

Among them, d_i is the original detail coefficient; λ is the threshold; d_i' is the processed detail coefficient. Soft thresholding can smoothly reduce the amplitude of wavelet coefficients, thereby reducing noise components in the signal while maintaining the main characteristics of the signal. This method can better protect the continuity of the signal.

Through the above filtering process, the obtained EMG signal is made purer, which facilitates subsequent analysis and research.

3.3. Model input and dynamic adjustment

In three-dimensional finite element analysis, using processed EMG as input parameters for the model plays a crucial role in driving the muscle units in the model. Firstly, the processed EMG signal needs to be converted into input parameters that the model can recognize and process in order to drive muscle units. The common method is to establish a relationship model between EMG and muscle stress.

In order to achieve dynamic adjustment of the model, this article adopts a PID controller to dynamically adjust the parameters of the finite element model. The PID controller dynamically adjusts the model parameters and boundary conditions through real-time collected biological signal feedback to ensure that the output of the model matches the actual physiological state. Assuming EMG $\mathrm{EMG(t)}$ is the input, its control signal $u(t)$ is shown in Equation (7).

$$u(t) = K_p[\mathrm{EMG}(t) - \mathrm{EMG_{ref}}] + K_i \int_0^{\mathrm{t}} [\mathrm{EMG}(\tau) - \mathrm{EMG_{ref}}]\,\mathrm{d}\tau + K_d \frac{\mathrm{d}}{\mathrm{d}t}[\mathrm{EMG}(t) - \mathrm{EMG_{ref}}] \tag{7}$$

Among them, $\mathrm{EMG_{ref}}$ is the reference EMG value, and K_p, K_i, and K_d are the proportional, integral, and differential gain coefficients, respectively.

The control signal is input into the finite element model and the material properties of the model are adjusted. Due to the use of the Ogden model to describe the nonlinear elastic behavior of muscle tissue, the material properties of the model are updated through real-time feedback. Cartilage tissue is described for its mechanical properties using a linear elastic model, and the material properties of the model are represented by a stress-strain relationship. The adjustment of the Young's modulus E and Poisson's ratio ν of the material is shown in Equations (8) and (9).

$$E(t) = E_0 + K_E u(t) \tag{8}$$

$$\nu(t) = \nu_0 + K_\nu u(t) \tag{9}$$

Among them, E_0 and ν_0 are initial values, and K_E and K_ν are control gains.

The boundary conditions of the model are adjusted based on real-time feedback of biological signals using Equation (10).

$$\begin{aligned} K &= K_0 + \Delta K \\ C &= C_0 + \Delta C \\ M &= M_0 + \Delta M \end{aligned} \tag{10}$$

Among them, K_0, C_0, and M_0 are the initial stiffness matrix, damping matrix, and mass matrix, respectively, while ΔK, ΔC, and ΔM are the dynamic adjustment quantities based on real-time biological signal feedback.

By using the processed EMG signal as an input parameter and utilizing PID control algorithm to dynamically adjust the model parameters, the mechanical behavior of the vocal mechanics model can be effectively simulated and optimized, providing new methods and technical support for personalized medical diagnosis and treatment. In the process of using a PID controller for dynamic adjustment, the Ziegler Nichols rule is first used for preliminary parameter tuning. When the proportional gain Kp is set to 0.5, the system begins to oscillate with an oscillation period of Tp = 2 seconds. Calculate the initial parameters of the PID controller according to the Ziegler Nichols rule. Among them, the proportional gain is 0.3, the integral gain is 0.18, and the differential gain is 0.075. Test the response of the system under different vocal states (monosyllabic pronunciation, speech, singing), and record the response time and stability of the system. If the system response is too slow, gradually increase the proportional gain. If there is steady-state error in the system, gradually increase the integral gain to ensure that the PID controller can effectively control the system response during dynamic adjustment.

Hexahedral meshes usually provide higher accuracy and stability when simulating solid structures, so this article uses hexahedral meshes for mesh partitioning. To ensure that the model can accurately capture the complex geometric features of the vocal cords and throat, the basic mesh size is first determined to be 1mm. Perform local mesh refinement in key areas such as vocal cords and larynx. The grid size of the vocal cord area will be refined to 0.5mm. Refine the throat area locally, with a grid size of 0.5mm.

Using adaptive grid partitioning technology, dynamically adjust the grid density based on the distribution of stress or strain during the simulation process. Ensure that the generated mesh meets quality standards, with a minimum angle of no less than 20 degrees and a maximum distortion of no more than 0.8.

The vocal cords are mainly composed of elastic fibers, with a selected elastic modulus of 500 kPa and Poisson's ratio of 0.45. The elastic modulus of muscles is generally between 1 kPa and 100 kPa. Considering the characteristics of the throat muscles, an elastic modulus of 50 kPa and a Poisson's ratio of 0.5 were chosen. To simulate the structure of laryngeal cartilage, an elastic modulus of 5 MPa and a Poisson's ratio of 0.45 were selected. The elastic modulus of the mucosa is 0.5 kPa, and the Poisson's ratio is 0.45. The interface properties between vocal cords and surrounding tissues need to consider friction coefficient and adhesion force. Set the friction coefficient between the vocal cords and the soft tissues of the throat to 0.2.

Enter the above material properties in finite element analysis software to ensure that each tissue type has corresponding property values. Choose a linear elastic model to simulate the behavior of biological tissues.

3.4. Sound simulation and mechanical properties

The vocal cords, the most important part of vocalization, are simulated and analyzed. **Figure 4** shows a three-dimensional geometric model simulation image of

the opening and closing of the vocal cords during the vocalization process.

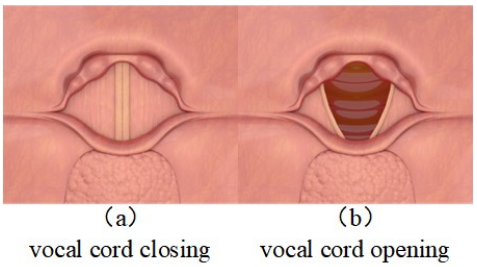

Figure 4. Three-dimensional geometric model simulation of vocal cord opening and closing. **(a)** vocal cord closing; **(b)** vocal cord opening.

Vocal cord vibration analysis is the key to understanding the mechanical properties during the process of vocalization. By combining collected biological signals to simulate the vibration behavior of vocal cords, how biological signals affect the dynamic properties of vocal cords is revealed. Modal analysis method is used to simulate the vibration mode of vocal cords and analyze their natural frequency and amplitude. Modal analysis is a method used to determine the dynamic properties of a system under natural vibration conditions.

The dynamic equation shown in Equation (3) is established, where the external force vector $f = 0$, indicating that there is no external force acting on the system, that is, the system is in a state of natural vibration. Ignoring the damping term, a simplified eigenvalue problem can be obtained, as shown in Equation (11).

$$(K - \omega^2 M)u = 0 \tag{11}$$

The eigenvalue ω^2 and corresponding eigenvector u of the system are obtained by solving the equation. The eigenvalue ω^2 corresponds to the natural frequency of the system, and the eigenvector u corresponds to the mode shape of the system.

Based on the eigenvalues and eigenvectors, the natural frequency and vibration mode of the vocal cords are determined. **Figure 5** shows the vibration patterns of the vocal cords at different frequencies, providing a visual representation for understanding the mechanical properties of the vocal cords.

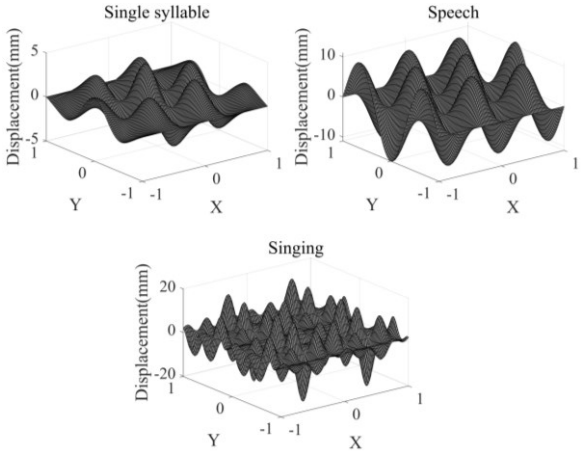

Figure 5. Vibration mode diagram of different sound states.

The vibration frequency and amplitude of the vocal cords vary among single syllable vocalization, normal speech, and singing. By comparing the vibration patterns under different vocal states, it can be seen that the frequency is lower and the harmonic components are less in the single syllable vocal state; under normal speech conditions, the frequency is high and there are many harmonic components; when singing, the frequency is the highest and the harmonic components are the most complex. This reflects the differences in vocal cord vibration characteristics under different vocal states.

To further analyze the acoustic mechanical properties, this article conducts simulation analysis on its key indicators (sound pressure distribution and resonance frequency). The sound pressure distribution is obtained by simulating the propagation of sound waves, reflecting the energy distribution of sound waves in the channel. The calculation of resonance frequency is based on the frequency response of the sound pressure field, which is obtained by extracting the frequency components of the sound pressure field through Fourier transform using Equation (12). The sound pressure distribution image and resonance frequency image are shown in **Figures 6** and **7**, respectively.

$$X[k] = \sum_{n=0}^{N-1} x\,[n]\mathrm{e}^{-j\frac{2\pi}{N}kn} \tag{12}$$

Among them, $X[k]$ is the k-th frequency component in the frequency domain; $x[n]$ is the n-th sample value in the time domain; N is the total number of samples in the signal; j is an imaginary unit.

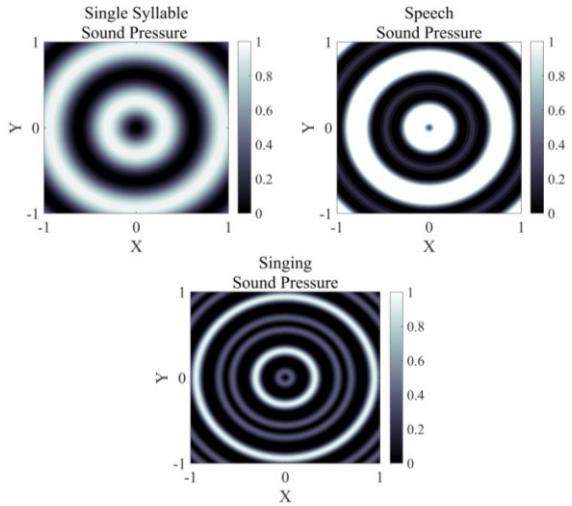

Figure 6. Sound pressure distribution diagram for different sound states

The sound pressure distribution results show significant differences in sound pressure distribution under different sound states. In the single syllable sound state, the color transition of the sound pressure image is natural, that is, the sound pressure distribution is uniform; under normal speech conditions, the sound pressure image forms multiple highlighted areas, indicating the presence of high-pressure regions; in the singing state, the sound pressure image forms distinct resonant cavities (areas with obvious shapes and large color changes) and nodes (large areas with darker colors).

These high-pressure regions and resonant cavities also reflect the existence of resonance phenomena.

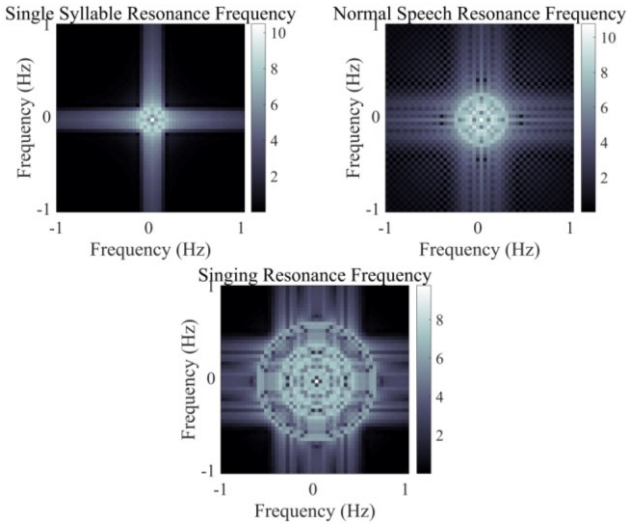

Figure 7. Resonance frequency diagram of different vocal states.

The resonance frequency results show that the resonance frequency of single syllable vocalization is concentrated in the low-frequency region; under normal speech conditions, the resonance frequency range is wide and contains multiple frequency components; when singing, the resonance frequency range is the largest and the frequency distribution pattern is the most complex. These resonance frequencies reflect the main frequency components and propagation characteristics of vocal cord vibration.

4. Model performance evaluation and real-time performance

4.1. Model performance evaluation

In order to evaluate the reliability of the constructed three-dimensional finite element model, this article compares the simulated data of the model with experimental data, and comprehensively evaluates the reliability of the model through two quantitative evaluation methods: correlation coefficient and root mean square error. These two methods can effectively measure the consistency and accuracy of the model with experimental data, providing clear directions for model improvement. The collected and preprocessed EMG data is used as input to drive a three-dimensional finite element model for simulation.

A total of 15 participants were recruited for this experiment, ranging in age from 20 to 50 years old, with an average age of 35 years old. This age group covers early to middle adulthood, with 8 males and 7 females among the participants, with a gender ratio close to 1:1, ensuring that the experimental results are not significantly affected by gender factors. All participants were confirmed by medical examination to have no hearing impairment, vocal cord disease, or other health issues that may affect their vocal ability. Special attention was paid to excluding smokers to reduce the potential impact of tobacco use on experimental results.

The output of the model simulation includes the displacement time series of vocal cord vibration, sound pressure distribution, and resonance frequency under different vocal states. The correlation coefficient and root mean square error (RMSE) are used to quantitatively evaluate the consistency and accuracy between the model simulation results and experimental data. The specific data is shown in **Table 2**.

Table 2. Statistical table of correlation coefficient and root mean square error

Vocalization State		Vocal Cord Vibration Correlation Coefficient	Vocal Cord Vibration RMSE	Sound Pressure Distribution Correlation Coefficient	Sound Pressure Distribution RMSE	Resonance Frequency Correlation Coefficient	Resonance Frequency RMSE
Single Syllable	Left SCM	0.9123	0.1534	0.8765	0.2047	0.9432	0.1045
	Right SCM	0.9054	0.1578	0.8845	0.1983	0.9517	0.1098
	Cricothyroid	0.8947	0.1459	0.8921	0.2105	0.9589	0.1153
Speech	Left SCM	0.8798	0.1845	0.8521	0.2473	0.8965	0.1221
	Right SCM	0.8834	0.1812	0.8476	0.2539	0.9024	0.1187
	Cricothyroid	0.8712	0.1876	0.8583	0.2445	0.8941	0.1265
Singing	Left SCM	0.9538	0.0987	0.9165	0.1523	0.9754	0.0843
	Right SCM	0.9491	0.1032	0.9238	0.1487	0.9712	0.0876
	Cricothyroid	0.9617	0.0954	0.9112	0.1576	0.9786	0.0809

For each set of data, the correlation coefficient ranges from −1 to 1, with values closer to 1 indicating higher consistency between the model and experimental data. The smaller the root mean square error, the closer the model simulation results are to the experimental data. From the data in **Table 1**, it can be found that the simulated results of vocal cord vibration, sound pressure distribution, and resonance frequency under different vocal states of the model have high consistency and small errors with experimental data. The correlation coefficient is mostly above 0.85, and only the correlation coefficient of sound pressure distribution when speaking normally at the right sternocleidomastoid muscle is 0.8476, which is less than 0.85. The RMSE coefficient is mostly within 0.2, but there are also 5 groups of data that exceed 0.2. The overall level is good but the level is poor compared to the correlation coefficient data. Among them, the RMSE data of the 3 groups in normal speech state is significantly higher than that in single syllable vocalization and singing state, which may be due to the larger range of normal speech and more influencing factors. The above data indicates that the model can accurately simulate the biomechanical properties under different vocal states, which has high reliability.

To understand the robustness and adaptability of the model, this article collected electromyographic signal data from different individuals, and selected a representative group of participants, including individuals of different genders, ages, and occupational backgrounds, to cover a wide range of vocal cord usage. The basic information of the participants is shown in **Table 3**:

Table 3. Basic information of participants.

Participant sequence	Gender	Age	Professional background	Sound type	Health condition
P1	Male	27	Singer	High pitch	Healthy
P2	Female	35	Teacher	Middle pitch	Healthy
P3	Male	42	Lawyer	Low pitch	Healthy

The experimental data of different individuals are shown in **Table 4**:

Table 4. Experimental data from different individuals.

Participant	Phonation modes	Correlation coefficient	RMSE (Pa)	Resonance frequency error (Hz)
P1	Single Syllable	0.8507	0.1277	2.5311
	Speech	0.8021	0.1061	4.0216
	Singing	0.7533	0;1258	6.3349
P2	Single Syllable	0.8279	0.1232	3.0527
	Speech	0.7801	0.1547	4.6173
	Singing	0.7325	0.1559	7.1548
P3	Single Syllable	0.8882	0.1492	1.5296
	Speech	0.8401	0.1022	3.5355
	Singing	0.8036	0.1339	5.5179

Overall, from **Table 4**, the model performs the best in simulating simple vocal states (such as monosyllabic sounds), while still maintaining a certain level of accuracy when dealing with more complex vocal activities (such as speech and singing).

To evaluate the accuracy of the model, this study compares the simulation results with experimental data and calculates the relative error to assess the accuracy of the model under different vocal states. The relative error distribution of different vocal states is shown in **Figure 8**.

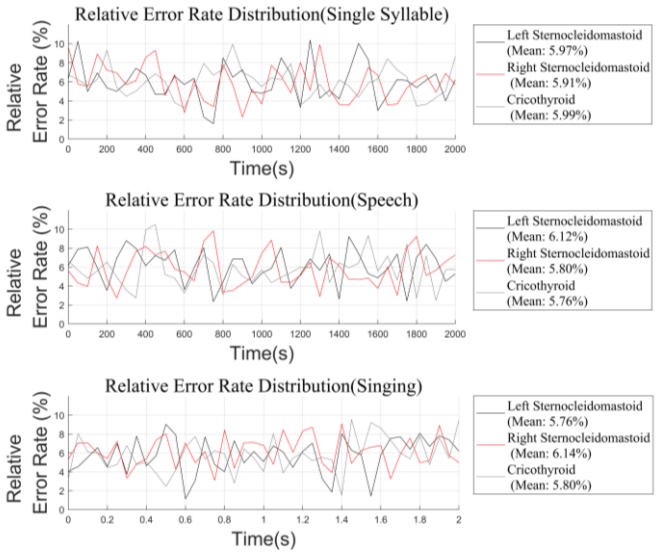

Figure 8. Distribution of relative error.

The results show that the average relative error data between the simulation results and experimental data of the model in different vocal states are mostly within 6%, which is at a good level. Among them, only two groups have an average relative error data exceeding 6%, proving that the model has high accuracy overall.

4.2. Real-time performance of the model

To evaluate the real-time feedback capability of the model, this article records the feedback delay time from signal acquisition to model adjustment in real-time, calculates the minimum and maximum feedback delay times, calculates the corresponding average feedback delay time and standard deviation, and analyzes the feedback delay level and dispersion degree of the simulated data of the model. The specific statistical analysis data is shown in **Table 5**.

Table 5. Real-time analysis table.

Vocalization State		Minimum Feedback Delay (ms)	Maximum Feedback Delay (ms)	Average Feedback Delay (ms)	Standard Deviation
Single Syllable	Left SCM	45	85	63	9.21
	Right SCM	48	90	66	11.12
	Cricothyroid	42	82	60	8.31
Speech	Left SCM	62	126	92	13.20
	Right SCM	65	103	87	12.52
	Cricothyroid	59	95	79	12.02
Singing	Left SCM	38	80	58	10.06
	Right SCM	41	83	61	11.40
	Cricothyroid	37	78	55	9.53

The data in **Table 5** shows that the total average feedback delay time of the three sets of data in single syllable vocalization state is 63 milliseconds; the total average feedback delay time of the three sets of data in normal speech state is 86 milliseconds; the total average feedback delay time of the three sets of data in singing state is 58 milliseconds. The average feedback delay time of the system in all sound states is less than 100 milliseconds, which is generally at a good level. In terms of standard deviation, the standard deviation data under normal speech state is significantly higher than that under single syllable vocalization and singing state, indicating that the feedback delay fluctuation is the largest under normal speech state. The feedback delay in single syllable vocalization and singing states is relatively stable, which may be due to the more variable vibration patterns of the vocal cords in normal speech states compared to single syllable vocalization and singing states. The above conclusion indicates that the model has good real-time feedback capability.

5. Conclusions

This article was based on a three-dimensional finite element analysis method using biological signal feedback. By collecting and processing individual EMG in real-time as input parameters for the finite element model, the mechanical properties of sound production were simulated, and a PID controller was used to dynamically

adjust the model. The vocal cord vibration, including vocal cord vibration mode analysis, sound pressure distribution analysis, and resonance frequency analysis, was simulated and analyzed. By comparing and analyzing simulated data with collected data, the results showed that the model had a low error rate. Analyzing the real-time feedback capability of the system, the results indicated that the system had high real-time performance. The above conclusions verified the reliability and practicality of the model, providing theoretical and technical support for personalized medical diagnosis and treatment. However, this article also has limitations as three-dimensional finite element analysis typically requires a significant amount of computational resources to solve complex partial differential equations. In real-time applications, fast computing speed is essential. In future research, we will consider improving computational performance and shortening computation time to promote the high-quality development of biological signal feedback.

Funding: This study was supported by the China National University Student Innovation & Entrepreneurship Development Program (S202312034016), the 14th Five-Year Plan of Education Research Development in Hunan Province (ND213721), Philosophy and Social Science Funds project in Hunan Province (18YBQ034).

Ethical approval: Not applicable.

Conflict of interest: The author declares no conflict of interest.

References

1. Glazier PS, Mehdizadeh S. Challenging Conventional Paradigms in Applied Sports Biomechanics Research. Sports Medicine. 2018; 49(2): 171-176. doi: 10.1007/s40279-018-1030-1
2. Willy RW, Paquette MR. The Physiology and Biomechanics of the Master Runner. Sports Medicine and Arthroscopy Review. 2019; 27(1): 15-21. doi: 10.1097/jsa.0000000000000212
3. Odom KJ, Araya-Salas M, Morano JL, et al. Comparative bioacoustics: a roadmap for quantifying and comparing animal sounds across diverse taxa. Biological Reviews. 2021; 96(4): 1135-1159. doi: 10.1111/brv.12695
4. Yang S, Liu Y, Ma S, et al. Stress and strain changes of the anterior cruciate ligament at different knee flexion angles: A three-dimensional finite element study. Journal of Orthopaedic Science. 2024; 29(4): 995-1002. doi: 10.1016/j.jos.2023.05.015
5. Kilic E, Doganay O. Evaluation of Stress in Tilted Implant Concept With Variable Diameters in the Atrophic Mandible: Three-Dimensional Finite Element Analysis. Journal of Oral Implantology. 2020; 46(1): 19-26. doi: 10.1563/aaid-joi-d-19-00066
6. Oh JH, Kim YS, Lim JY, et al. Stress Distribution on the Prosthetic Screws in the All-on-4 Concept: A Three-Dimensional Finite Element Analysis. Journal of Oral Implantology. 2020; 46(1): 3-12. doi: 10.1563/aaid-joi-d-19-00090
7. Huang J, Ong SK, Nee AY. An approach for augmented learning of finite element analysis. Computer Applications in Engineering Education. 2019; 27(4): 921-933. doi: 10.1002/cae.22125
8. Onyibo EC, Safaei B. Application of finite element analysis to honeycomb sandwich structures: a review. Reports in Mechanical Engineering. 2022; 3(1): 283-300. doi: 10.31181/rme20023032022o
9. Papadopoulos K, Vintzileou E, Psycharis IN. Finite element analysis of the seismic response of ancient columns. Earthquake Engineering & Structural Dynamics. 2019; 48(13): 1432-1450. doi: 10.1002/eqe.3207
10. Palaparthi A, Smith S, Mau T, et al. A computational study of depth of vibration into vocal fold tissues. The Journal of the Acoustical Society of America. 2019; 145(2): 881-891. doi: 10.1121/1.5091099
11. Kusel ET, Siderius M. Comparison of Propagation Models for the Characterization of Sound Pressure Fields. IEEE Journal of Oceanic Engineering. 2019; 44(3): 598-610. doi: 10.1109/joe.2018.2884107
12. Alshoaibi AM. Finite element-based model for crack propagation in linear elastic materials. Engineering Solid Mechanics.

2020: 131-142. doi: 10.5267/j.esm.2019.10.002
13. Mohamed N, Eltaher MA, Mohamed SA, et al. Energy equivalent model in analysis of postbuckling of imperfect carbon nanotubes resting on nonlinear elastic foundation[J]. Structural Engineering and Mechanics, An Int'l Journal. 2019; 70(6): 737-750.
14. Nsugbe E. Brain-machine and muscle-machine bio-sensing methods for gesture intent acquisition in upper-limb prosthesis control: a review. Journal of Medical Engineering & Technology. 2021; 45(2): 115-128. doi: 10.1080/03091902.2020.1854357
15. Gohel V, Mehendale N. Review on electromyography signal acquisition and processing. Biophysical Reviews. 2020; 12(6): 1361-1367. doi: 10.1007/s12551-020-00770-w
16. Aly H, Youssef SM. Bio-signal based motion control system using deep learning models: a deep learning approach for motion classification using EEG and EMG signal fusion. Journal of Ambient Intelligence and Humanized Computing. 2021; 14(2): 991-1002. doi: 10.1007/s12652-021-03351-1
17. Tankisi H, Burke D, Cui L, et al. Standards of instrumentation of EMG. Clinical Neurophysiology. 2020; 131(1): 243-258. doi: 10.1016/j.clinph.2019.07.025
18. Bird JJ, Pritchard M, Fratini A, et al. Synthetic Biological Signals Machine-Generated by GPT-2 Improve the Classification of EEG and EMG Through Data Augmentation. IEEE Robotics and Automation Letters. 2021; 6(2): 3498-3504. doi: 10.1109/lra.2021.3056355
19. Rossi F, Mongardi A, Ros PM, et al. Tutorial: A Versatile Bio-Inspired System for Processing and Transmission of Muscular Information. IEEE Sensors Journal. 2021; 21(20): 22285-22303. doi: 10.1109/jsen.2021.3103608
20. Chai CP. Comparison of text preprocessing methods. Natural Language Engineering. 2022; 29(3): 509-553. doi: 10.1017/s1351324922000213
21. Jeong SW, Lee TH, Lee J. Frequency- and Bandwidth-Tunable Absorptive Bandpass Filter. IEEE Transactions on Microwave Theory and Techniques. 2019; 67(6): 2172-2180. doi: 10.1109/tmtt.2019.2914111
22. Merikangas KR, Swendsen J, Hickie IB, et al. Real-time Mobile Monitoring of the Dynamic Associations Among Motor Activity, Energy, Mood, and Sleep in Adults With Bipolar Disorder. JAMA Psychiatry. 2019; 76(2): 190. doi: 10.1001/jamapsychiatry.2018.3546
23. Curtis SD, Ploense KL, Kurnik M, et al. Open Source Software for the Real-Time Control, Processing, and Visualization of High-Volume Electrochemical Data. Analytical Chemistry. 2019; 91(19): 12321-12328. doi: 10.1021/acs.analchem.9b02553
24. Verma B, Padhy PK. Indirect IMC-PID controller design. IET Control Theory & Applications. 2019; 13(2): 297-305. doi: 10.1049/iet-cta.2018.5454
25. Elsisi M. Optimal design of non-fragile PID controller. Asian Journal of Control. 2019; 23(2): 729-738. doi: 10.1002/asjc.2248
26. Guan Z, Yamamoto T. Design of a Reinforcement Learning PID Controller. IEEJ Transactions on Electrical and Electronic Engineering. 2021; 16(10): 1354-1360. doi: 10.1002/tee.23430
27. Kench S, Cooper SJ. Generating three-dimensional structures from a two-dimensional slice with generative adversarial network-based dimensionality expansion. Nature Machine Intelligence. 2021; 3(4): 299-305. doi: 10.1038/s42256-021-00322-1
28. Song C, Alkhalifah T, Waheed UB. Solving the frequency-domain acoustic VTI wave equation using physics-informed neural networks. Geophysical Journal International. 2021; 225(2): 846-859. doi: 10.1093/gji/ggab010
29. Yang X, Tenreiro Machado JA. A new fractal nonlinear Burgers' equation arising in the acoustic signals propagation. Mathematical Methods in the Applied Sciences. 2019; 42(18): 7539-7544. doi: 10.1002/mma.5904
30. Wishart DS. Metabolomics for Investigating Physiological and Pathophysiological Processes. Physiological Reviews. 2019; 99(4): 1819-1875. doi: 10.1152/physrev.00035.2018
31. Lee J, Zhang XL. Physiological determinants of VO2max and the methods to evaluate it: A critical review. Science & Sports. 2021; 36(4): 259-271. doi: 10.1016/j.scispo.2020.11.006
32. Jiang W, Zheng X, Xue Q. Influence of vocal fold cover layer thickness on its vibratory dynamics during voice production. The Journal of the Acoustical Society of America. 2019; 146(1): 369-380. doi: 10.1121/1.5116567
33. Zhang Z. Oral vibratory sensations during voice production at different laryngeal and semi-occluded vocal tract configurations. The Journal of the Acoustical Society of America. 2022; 152(1): 302-312. doi: 10.1121/10.0012365
34. Sharma A, Sharma I, Kumar A. Signal Acquisition and Time–Frequency Perspective of EMG Signal-based Systems and

Applications. IETE Technical Review. 2023; 41(4): 466-485. doi: 10.1080/02564602.2023.2265897

35. Kamel MA, Ibrahim K, El-Makarem Ahmed A. Vibration control of smart cantilever beam using finite element method. Alexandria Engineering Journal. 2019; 58(2): 591-601. doi: 10.1016/j.aej.2019.05.009
36. Guan W, Sun Y, Qi X, et al. Spinal biomechanics modeling and finite element analysis of surgical instrument interaction. Computer Assisted Surgery. 2019; 24(sup1): 151-159. doi: 10.1080/24699322.2018.1560086